This is a non-peer reviewed preprint submitted to EarthArXiv. It is under review in Hydrogeology Journal.

Assessing the potential of low transmissivity aquifers for ATES systems: a case study in Flanders (Belgium)

Luka Tas[1], David Simpson[2], Thomas Hermans[1]

[1]Laboratory for Applied Geology and Hydrogeology, Department of Geology, Ghent University, Ghent, Belgium

[2]Advanced Groundwater Techniques, Kontich, Belgium

Correspondence: Luka Tas <luka.tas@ugent.be>

ABSTRACT

The Member States of the European Union pledged to reduce greenhouse gas emissions by 80-95% by 2050. Shallow geothermal systems might substantially contribute by providing heating and cooling in a sustainable way through seasonally storing heat and cold in the shallow ground (<200m). When the minimum yield to install a cost-effective aquifer thermal energy storage (ATES) system cannot be met, borehole thermal energy storage (BTES), relying mostly on the thermal conductivity of the ground, is proposed. However, for large-scale applications, this requires the installation of hundreds of boreholes which entails a large cost and high disturbance of the underground. In such cases, ATES systems can nevertheless become interesting. In this contribution, we present a case study performed on a Ghent University campus, where the feasibility of ATES in an area with a low transmissivity was determined. The maximum yield of the aquifer was estimated at 5 m^3/h through pumping tests. Although this low yield was attributed to the fine grain size of the aquifer, membrane filtering index tests and long-term injection tests revealed that the clogging risk was limited. A groundwater model was used to optimize the well placement while limiting the risk of interactions between the wells resulting in a thermal breakthrough or flooding at the surface. It was shown that a well arrangement in a

checkerboard pattern was most effective to reach these objectives. Hence, for large-scale projects, a minimal CO_2 output might be reached using a (more cost-effective) ATES system even in low permeable sediments.

Keywords: geothermal systems – pumping/injection/well test – heat transport – low-permeability media – groundwater modeling

1 Introduction

Shallow geothermal systems have proven to be locally available, green, and renewable alternatives to fossil fuels both for cooling in summer and heating in winter (Perego et al., 2020). On average 0.5 kg of CO_2 per m^3 of pumped water can be saved (Fleuchaus et al., 2018). Implementing such systems in the building sector has the potential to significantly reduce global greenhouse gas emissions (European Commission, 2012, 2019; Ramos-Escudero et al., 2021). The currently rising energy costs favour the investment in sustainable energy sources. More specifically, geothermal energy is labelled the most attractive option according to Batac et al. (2022). Therefore, shallow geothermal systems might become even more cost-efficient in the near future (Batac et al., 2022).

For buildings with a high energy demand, aquifer thermal energy storage (ATES) systems are generally favored over borehole thermal energy storage (BTES) systems as the costs of the drilling becomes more important compared to the other costs (pipework, controls…). A BTES system for that kind of application would require the installation of tens to hundreds of boreholes. Both BTES and ATES systems make use of a heat pump to extract the heat out of the subsurface reservoir. BTES systems are closed-loop systems which use ground heat exchangers in the subsurface i.e. long loops through which water, sometimes mixed with an antifreeze, circulates (Fig. 1). Their capacity is mostly dependent on the thermal conductivity of the ground and its capacity for thermal recharge (Bayer et al., 2012; Hecht-Méndez, 2013;

Glassley, 2015). In contrast, the efficiency of ATES systems is mostly dependent on the hydraulic conditions (hydraulic conductivity and hydraulic gradient) in the aquifer. These are open-loop systems which extract and inject groundwater from an aquifer through a well (Bloemendal et al., 2015).

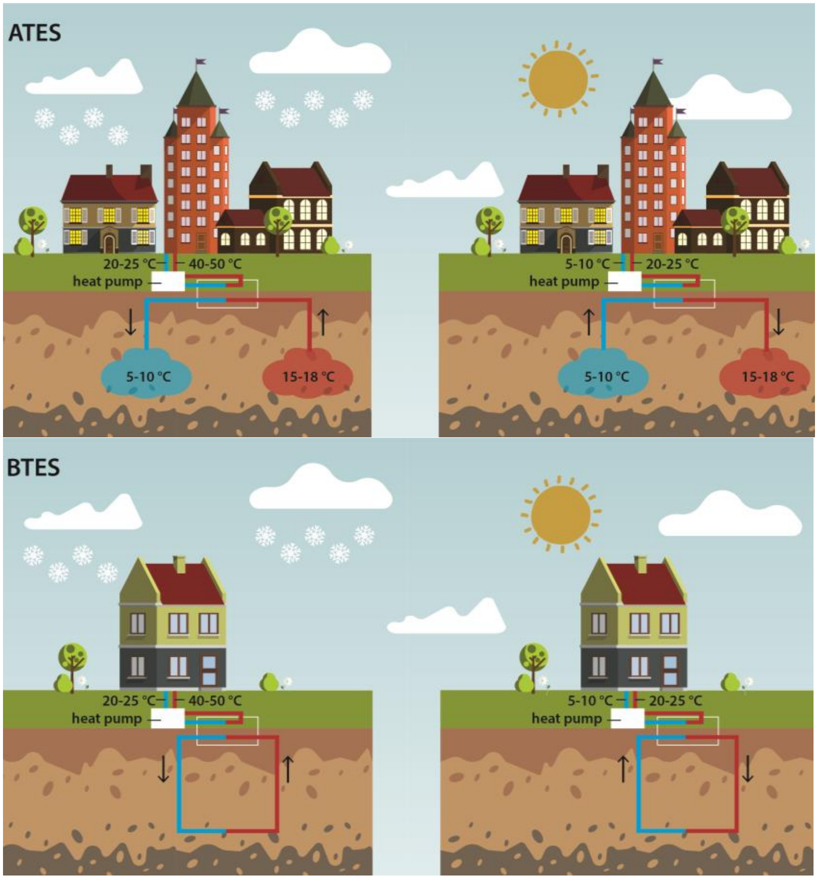

Fig. 1. Graphical representation of an ATES and BTES system in winter and summer season (after Bloemendal, 2018).

In Flanders, the potential of aquifer layers for installing ATES systems has been estimated based on their transmissivity (WTCB, 2017). When the transmissivity is below 50 m²/day, it is deemed unsuitable, while above 250 m²/d, the potential is recognized. In between those values further investigations are recommended. The threshold on the transmissivity implicitly accounts for the fact that a minimum yield of about 10 m³/h is required to justify the investment costs (Bloemendal et al., 2015; Hermans et al., 2018). Following these recommendations, the implementation of ATES systems was deemed unfeasible in many areas (Fig. 2). In these areas, BTES systems, which are less dependent on the variability of subsurface properties, are seen as the only viable option, even to fulfil a high power demand and therefore requiring significant investment costs and occupying significant surface areas (excluding areas of tree growth).

When such high investment costs are at play, it is nevertheless interesting to further explore the possibility of the development of an ATES system that would operate at limited pumping/injection rate per well (< 10 m^3/h). Since they produce more energy per well, they result in fewer, less deep drillings and hence a lower drilling cost. However, because of its dependence on aquifer properties, an ATES system is more complex and more prone to failure. For example, a reduction in injection capacity resulting from well clogging or thermal interference between warm and cold wells could result in reduced energy efficiency.

In this paper, we demonstrate the feasibility of an ATES system functioning at a low pumping rate (5 m^3/h) on Campus Sterre, Ghent University. This was accomplished by first estimating the maximum yield of the aquifer through pumping tests. In addition to this, considering the fine grain size of the aquifer, membrane filtering index (MFI) tests and long-term injection tests were carried out to estimate the clogging risk. For the actual ATES system, interactions between the wells might result in thermal breakthrough or flooding at the surface. To limit this risk, a groundwater model calibrated with the pumping test data was used to optimize the well placement.

2 Setting of the study area

Ghent University aims to become CO_2-neutral on the Faculty of Science campus (Campus Sterre) in Belgium by 2050. Reaching this scope is challenging and different sustainable, green, and innovative technologies should be studied and evaluated. Based on an energy audit, the most sustainable alternative to cover the heating and cooling demand on this campus was to combine the residual heat from cooling the servers with a shallow geothermal system. The geothermal system would store the residual heat of the servers during the summer period when heating is not needed, so it can be released in winter in addition to the directly used residual heat from the servers. The power of the geothermal buffer was estimated at 0.63 MW.

A quick evaluation of the study area showed that, because of the absence of a thick productive aquifer on campus, the transmissivity of the available aquifers might not be sufficient to reach a high enough pumping rate (Fig. 2). Alternatively, to cover the power demand in the study area, a BTES system of 175 boreholes of 100 m deep was proposed. As this would result in an investment cost of approximately € 3 500 000, and would result in large areas occupied by the borehole heat exchangers, it was decided to determine the potential for ATES.

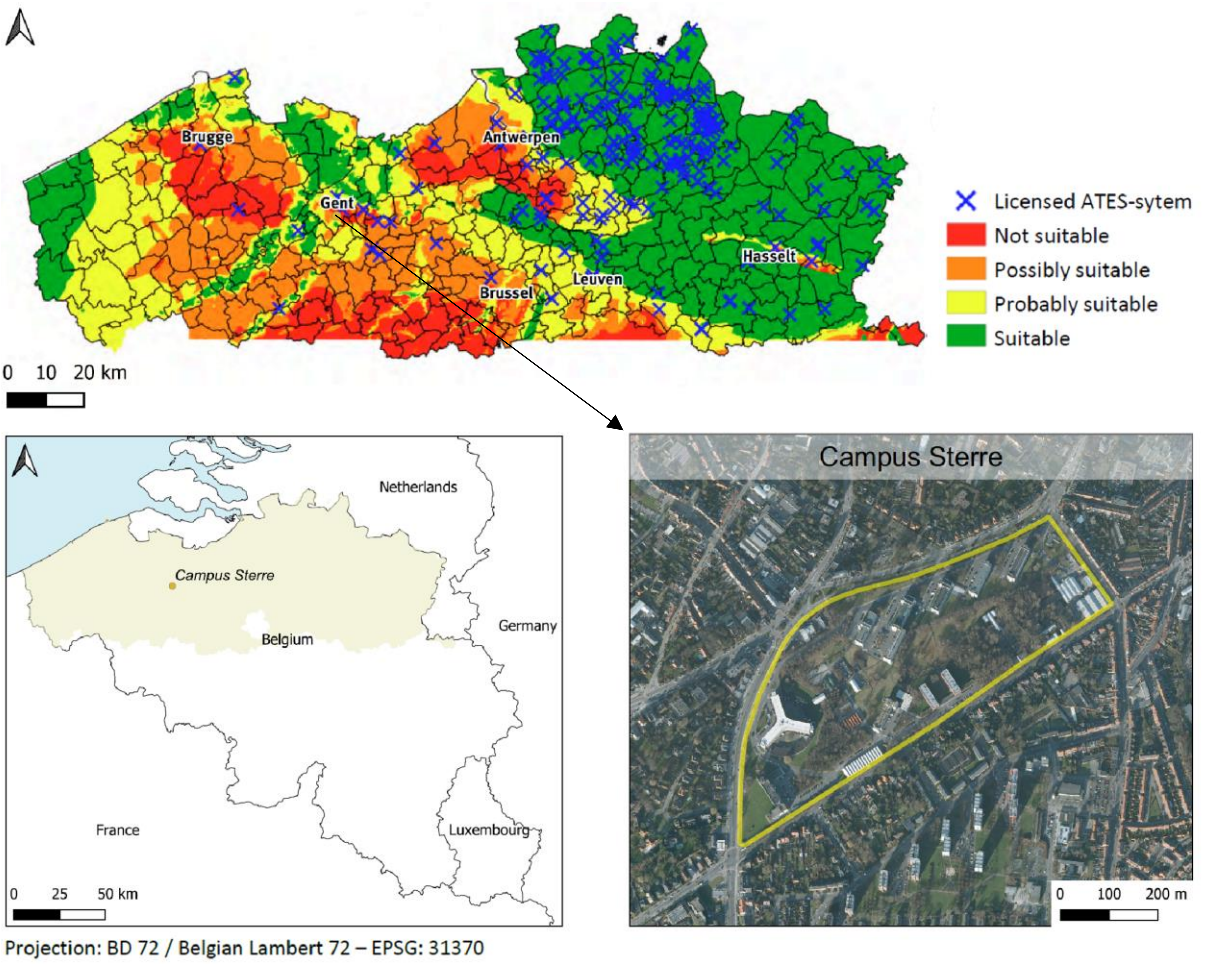

Fig. 2. Localization of the study area Campus Sterre on the suitability map for ATES systems in Flanders (Belgium) (after WTCB, 2017).

A description of the hydrogeology of the study area was made by Lebbe et al. (1992). Quaternary deposits, consisting of clays, silt, sand and gravel with a thickness of 9.5 m and variable hydraulic conductivity can be found at the surface. Below, the Formation (Fm) of Gentbrugge is considered a confining layer. It has an irregular extension: it thickens towards the Northeast and disappears in the Southwest of the study area. It is composed of silty clay or clayey silty glauconiferous very fine sand. Sand lenses with organic material and small pyritic concretions as well as layers of clayey sandy coarse silt might occur.

The main groundwater reservoir is situated below this formation. It has a uniform thickness of approximately 20 m and can be subdivided into 6 units according to Lebbe et al. (1992) (Fig. 3), labelled Yd 6 to Yd 1 from top to bottom. Yd 6 consists of slightly clayey glauconitic fine sand which might contain small shell fragments. The lithology of Yd 4 and Yd 2 resembles the one of Yd 6, without shell fragments. These three units are considered aquifer units. They have a cumulative thickness of 18.5 m, an average hydraulic conductivity of 1.08 m/day, and hence an average transmissivity of about 20 m^2/day. Yd 5, Yd 3 and Yd 1 contain more clay and are only semi-pervious: Yd 5 is very sandy clay, Yd 3 is sandy clay to clay, and Yd 1 is a sandy and silty clay with intercalations of thin clayey fine sand beds. This aquifer unit is bounded from -40 mTAW by the clayey Formation of Kortrijk, which is up to 95 m thick.

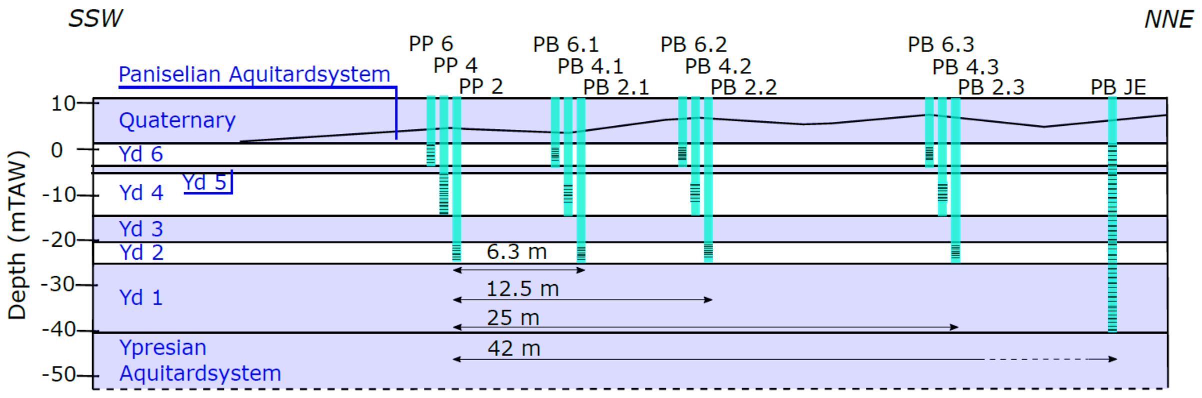

Fig. 3. Hydrostratigraphy across Campus Sterre with indication of the filter placement of the wells used for the pumping tests (created after DOV and Lebbe et al., 1992).

3 Methodology

3.1 Field tests

3.1.1 Pumping and injection

The efficiency of an ATES system relies on the hydraulic conductivity of the subsurface which governs the maximum pumping rate and the corresponding drawdown.

Lebbe et al. (1992) conducted a triple pumping test on Campus Sterre to determine the hydraulic parameters of the different layers. Pumping wells were drilled in the pervious layers Yd 2, Yd 4, and Yd 6 (named PP 2, PP 4 and PP 6 respectively). Each pumping well was accompanied by three observation wells located at fixed distances from the pumping well (Fig. 4).

Fig. 4. Localization of the well area used for the pumping tests on Campus Sterre.

Pumping tests were carried out in each pumping well separately. The pumping rate in PP 6, PP 4, and PP 2 was respectively 0.75 m^3/h, 3.09 m^3/h, and 1.66 m^3/h. The observation of the drawdown was done in all layers. Based on the results, the hydraulic conductivity and specific storage coefficient of the different layers were estimated through an inversion process (Lebbe et al., 1992).

For this study, additional field tests were carried out to:

1. Estimate the maximum pumping rate in the entire aquifer system. In absence of a fully filtered pumping well, this was estimated in each pervious layer separately. The total maximum pumping rate can be estimated by summing the individual rates if all pervious layers can be considered fully confined and independent of each other.
2. Estimate the maximum injection rate. For the injection test, a fully filtered well (PB JE) was used (Fig. 3). However, this well was constructed as a piezometer and has a limited inner diameter (63/57 mm). As such the well efficiency is not optimal limiting the injection capacity. Because the water level in the aquifer is shallow (~ 3 m below the surface), the injection might also cause water pressures above the ground level, potentially causing flooding and/or instability of the confining layer between Yd 6 and the top layer.
3. Simulate the long-term stability of a well pair consisting of one injection and one pumping well mimicking the behaviour of an ATES system.
4. Generate data sets for validation of the groundwater model.

In practice, the pumping and reinjection tests took place in the same wells that were used by Lebbe et al. (1992). Unfortunately, the three observation wells that accompanied pumping well PP 4 (PB 4.1, 4.2 and 4.3) were not accessible anymore. In August 2021 the maximum pumping rate in each pumping well was estimated.

To simulate the stability of a well pair, PP 4 was selected as the pumping well and PB JE as the injection well. Pressure transducers were installed in PP 2, PB 2.1, PP 4, PP 6, PB 6.1, PB 6.2 and PB JE to record the hydraulic head and temperature. In the pumping well, a probe measuring the electrical conductivity was also installed.

The actual pumping test started on October 25 2021, with a maximum estimated pumping and reinjection rate of 3.8 m^3/h in PP 4, based on the limited capacity of the injection well. The injection in PB JE started half an hour later. From 11h45 to 13h00, October 28, the pumping and injection were disturbed due to the execution of an MFI test (see section 3.1.2). The injection stopped on November 5 because of a failure in the pump and restarted at a slightly lower rate of 3.05 m^3/h until December 20.

3.1.2 Membrane Filtering Index

Because the aquifer contains fine particles, the (injection) wells could clog relatively rapidly. As a result, the injection pressure can increase over time and therefore decrease the injection capacity. For ATES systems, the wells are alternately injection or pumping wells according to the season. As such, if the capacity of the wells would decrease over time due to clogging, this would be detrimental to the overall efficiency and capacity of the ATES system (Jenne et al., 1992; De Zwart, 2007).

Therefore, a Membrane Filtering Index (MFI) test was carried out on-site to determine the clogging risk. It is a measure of the rate at which a filter paper (0.45 µm) becomes clogged under constant water pressure (2 bar) (Schippers & Verdouw, 1979, 1980; Olsthoorn, 1982). The index can be derived by plotting the ratio of the filtration time and the filtered sample volume (t/V) as a function of the total filtered volume (V). When the slope of the curve is inferior to 10, the water purity is considered acceptable for reinjection purposes for ATES systems. When the slope of the graph is lower than 3, the water purity is considered excellent for reinjection (Schippers & Verdouw, 1980; Olsthoorn, 1982). The actual MFI test for this study was carried out twice from 11h45 to 13h00 on October 28, 2021, after the well was sufficiently developed and the sand content (> 70 µm) of the pumped water was visually analysed (Aalten & Witteveen, 2015). Next, a long-term pumping and reinjection test (October 25 - December 20) served to verify whether there was a decrease in injection capacity with time.

3.2 Groundwater model

Because of the limited maximum yield of the aquifer, an ATES system would operate close to the maximum yield to minimize investment costs and several well pairs are therefore needed to fulfil the energy demand. The system must therefore be carefully designed to avoid hydraulic and thermal interaction between the wells. Creating a numerical model is a viable and indispensable tool to assess the feasibility of the project. It not only helps in understanding and predicting the behaviour of complex systems but it also helps to optimize the desired project implementation (Yapparova et al., 2014).

For this project, the freely available USGS MODFLOW 6 software was used (Langevin et al., 2017a, 2017b) together with the software ModelMuse as a graphical user interface (Winston, 2019). MODPATH was used to simulate advective transport (Pollock, 2012) and MT3D-USGS was used to model the full transport processes (Bedekar et al., 2016). MODFLOW 6 uses the control-volume finite-difference method to solve the mathematical equation numerically (Langevin et al., 2017a).

Based on the hydrostratigraphic setting of the study area in Fig. 3 and the already calibrated model parameters by Lebbe et al. (1992), a 3D model of 5 x 5 km around Campus Sterre was made (Table 1). All layers, except for the Quaternary, were set to be confined in the model. A structural grid was used for the spatial discretization (DIS package) (Langevin et al., 2017a). To improve the solution but avoid an exaggerated computation time, the grid was only refined where a steep gradient is expected, i.e. around the pumping/injection wells. The largest grid size was 100 m and was decreased to 5 m, 0.5 m and finally approximating the drilling diameter of the wells (roughly 0.25 m). For heat transport the smallest grid size was set to 1 m around the well area to limit the computational time. The previously smaller cell size was needed for calibration, assess the wellbore effect on the accuracy of the numerical model, and to limit numerical dispersion for the advective transport simulation.

Table 1. Hydraulic parameters used as input for the model (after Lebbe et al., 1992).

Layer	Top and bottom (mTAW)	*Kx* (m/s)	*Kz* (m/s)	*Ss* (1/m)	*Sy* (m^3/m^3)	Porosity
8 (Quaternary)	+10.4 to +2.4 (varying)	2,89E-06	4,73E-09	5,50E-05	9,84E-03	0,3
7 (Gentbrugge Fm.)	+2.4 (varying) to +1.4	2,89E-06	4,73E-09	5,50E-05	9,84E-03	0,3
6 (Yd 6)	+1.4 to -3.6	9,94E-06	5,79E-06	5,50E-05	9,84E-03	0,3
5 (Yd 5)	-3.6 to -5.1	2,31E-07	2,44E-07	5,50E-05	9,84E-03	0,3
4 (Yd 4)	-5.1 to -14.6	1,28E-05	1,13E-05	3,60E-05	9,84E-03	0,3
3 (Yd 3)	-14.6 to -20.6	2,31E-08	8,61E-09	3,60E-05	9,84E-03	0,3
2 (Yd 2)	-20.6 to -24.6	1,46E-05	1,14E-08	3,80E-05	9,84E-03	0,3
1 (Yd 1)	-24.6 to -40.6	4,63E-07	3,11E-07	1,20E-05	9,84E-03	0,3

For the bottom of the model, a no-flow boundary was set, as below Yd 1 the aquitard corresponding to the Kortrijk Fm is present. The Northern, Eastern, Southern and Western boundaries were set as constant head boundaries with a hydraulic head of +10 mTAW for the calibration period. For the long-term simulations, a hydraulic gradient of 0.14%, deduced from monitoring wells located outside of the study area, was imposed. At the start of each simulation, an initial head of +6.97 mTAW was chosen. This is the hydraulic head that was measured in PP 4 before the installation of the diver in October 2021. Zero-dispersion/diffusion heat flux was imposed for the transport boundary conditions. Only transient simulations were used, because of the interest in the evolution of the groundwater level/ thermal storage with time.

Heat transport can be translated into a mathematical problem using the following equation (Zheng, 2010):

$$\left(1+\frac{1-\theta_t}{\theta_t}\frac{\rho_s}{\rho_w}\frac{c_s}{c_w}\right)\frac{\partial(\theta_t T)}{\partial t}=\nabla\left(\theta_t\left(\frac{k_0}{\theta_t\rho_w c_w}+D_{mech}\right)\times\nabla T\right)-\nabla(qT)+q_s T_s \qquad \{1\}$$

$$with \qquad k_0 = k_w\theta + k_s(1-\theta)$$

$$\rho_b = \rho_s(1-\theta_t)$$

Table 2. Overview of the parameters used in the heat transport equation.

θt	total porosity [%]	35
ρb	bulk density [kg/m^3]	1716
t	time [s]	-
q	specific discharge vector [m/s]	-
qs	volumetric flow rate per unit volume of the aquifer representing sources or sinks [m/s]	-
ρs	density of the solid [kg/m^3]	2640
ρw	density of the water [kg/m^3]	1000
cs	specific heat capacity of the solid [J/(kg°C)]	710
cw	specific heat capacity of the water [J/(kg°C)]	4183
T	temperature [°C]	-
$k0$	bulk thermal conductivity [W/(m°C)]	2.153
kw	thermal conductivity of the water [W/(m°C)]	0.58
ks	thermal conductivity of the solid [W/(m°C)]	3
$Dmech$	mechanical dispersion coefficient tensor [m^2/s]	-
Ts	source temperature	-

The parameters of equation 1 and their values are defined in Table 2. The latter are the ones used by Vandenbohede et al. (2011) in a shallow heat injection and storage experiment performed in the Quaternary layer. They represent typical values of quartz sediment (Langevin et al., 2007). Since thermal parameters have a smaller range than hydraulic conductivity, they can be considered representative of the aquifer.

Because of the similarity between solute and heat transport and because of the disregarding of density/viscosity effects, MT3D-USGS can be used to model heat transport processes (Zheng, 2010; Hecht-Méndez et al., 2010; Sommer et al., 2013; Possemiers, 2014). The heat transport by conduction and thermal dispersion is analogous to molecular diffusion and mechanical dispersion in the solute transport equation. Next, the transport of heat by groundwater flow is analogous to the advection term in the solute transport equation (Zheng, 2010). To implement this in MT3D-USGS, the (thermal) distribution coefficient (K_d^t) and the molecular diffusion coefficient (D_m^t) must be defined as follows (Zheng, 2010):

$$K_d^t = \frac{c_s}{c_w \rho_w} = 1.69 * 10^{-4}\ m^3/kg \qquad D_m^t = \frac{k_0}{\theta_t \rho_w c_w} = 1.47 * 10^{-6}\ m^2/s \qquad \{2\ and\ 3\}$$

To solve the heat transport equation, the third-order TVD (Total Variation Diminishing) method with a backward approximation was used (Zheng and Wang, 1999). We also tested the Method of Characteristics (MOC), which simulates more gradually thermal diffusion, however it did not change our conclusions. The Generalized Conjugate Gradient (GCG, convergence criterion of 10^{-10}) Solver was used to implicitly solve the dispersion, sink/source and reaction terms with a finite-difference method. Finally, a linear sorption isotherm was selected in the RCT package. It accounts for the heat transfer process between the fluid and the solid (conduction).

The heat transfer process between the fluid and the solid (conduction) results in a retardation of the movement of the warm/cold temperature plume in comparison to the average linear groundwater flow velocity (Zheng and Wang, 1999; Vandenbohede et al., 2011).

$$thermal\ retardation\ factor = 1 + \frac{\rho_b}{\theta} K_d^t = 1.83 \qquad \{4\}$$

It is assumed that the transfer of heat from the mobile groundwater to the immobile pore water and the solid fraction is fast enough to be negligible compared to the flow velocity of the mobile groundwater. This assumption combined with a linear sorption model allows to combine the mobile and immobile water in one total porosity.

Model calibration is needed to ensure that the model will approximate the reality as closely as possible. In practice, because Lebbe et al. (1992) gathered a lot of valuable data in the study area, the values of their already calibrated model were used to first simulate the triple pumping test with the newly constructed model. In essence, the resulting drawdowns of these field tests were compared to the simulated ones aiming for a good agreement. Following this, the pumping/injection test was simulated to validate the model.

3.3 Model scenario

To design an ATES system, first the energy demand of the building, both for heating and cooling, that must be fulfilled by geothermal energy must be determined. With this knowledge, the total volume of water to be extracted can be estimated based on the heat capacity of water. This is illustrated by the following equations, ignoring the coefficient of performance of the heat pump (Glassley, 2015):

$$E = V \times c \times \Delta T \qquad Q = \frac{V}{t} \leftrightarrow Q = \frac{E}{tc\Delta T} = \frac{P}{c\Delta T} \qquad \{5\}$$

where E (J) is the thermal energy that can be stored/extracted from a given volume of water V (m^3), c *is* the volumetric heat capacity of water ($4.178 \cdot 10^6$ J/m^{3}K), ΔT the temperature difference between the extracted and injected water (K), Q the total flowrate of the system (m^3/s), t the time (s), and P the power (W). As such, knowing the maximum pumping/injection rate for a single well pair, the required number of well pairs can be calculated.

Knowing the number of wells, optimal use of (sub)surface space and optimal storage efficiency should be realized. One of the parameters influencing this performance, besides the groundwater flow and pumping rate, is the well placement (Yapparova et al., 2014). Many studies have been carried out related to this topic. In short, it was shown that storage efficiency decreases with decreasing distance between the warm and cold well areas. The storage efficiency also decreases with increasing hydraulic conductivity (Kim et al., 2010; Yapparova et al., 2014). As such, the relatively low hydraulic conductivity in the study area might be an advantage in this project which can be used to choose a smaller distance between the wells. Hence, optimizing the usage of space without compromising on storage efficiency. The fact that the storage efficiency decreases with increasing hydraulic conductivity can be explained by a short circuit between the cold and warm well areas. This is also often called a thermal breakthrough, resulting in a gradual attenuation of the ATES efficiency (Kim et al., 2010; Gao et al., 2013; Yapparova et al., 2014; Bloemendal et al., 2018). In theory, it is sufficient to ensure that the distance between the cold and warm wells in the design of the system is sufficient. This safe distance can be estimated from the thermal radius of influence (R_{th}) (Bloemendal et al., 2018; Bloemendal and Olsthoorn, 2018). The distance between wells of the opposite and same type should be $2.5 \cdot R_{th}$ and $1 \cdot R_{th}$ respectively. To apply this formula in practice, first, the hydraulic radius of influence was estimated analytically using the Thiem-Dupuit method for a confined aquifer in steady-state (Dupuit, 1863, Thiem, 1906):

$$R = 10^{\frac{s \times 2\pi K e}{Q}} \times x \qquad \{6\}$$

where R is the hydraulic radius of influence (m), s the drawdown at a certain distance x (m) from the well due to pumping/injecting (m), K is the horizontal hydraulic conductivity of the medium (m/s), e the thickness of the groundwater reservoir (m), and Q the pumping/injection rate (m^3/s). Finally, using the earlier defined thermal retardation factor, the thermal radius of influence (R_{th} = hydraulic radius / thermal retardation factor) can be estimated.

While the clustered well placement (i.e. a group of wells of the same type) might be a better option considering the storage efficiency, the opposite (i.e. alternating injection and pumping wells) might be beneficial for the hydraulic head. The latter must also be taken into account as, on the one hand, it must be able to maintain a low enough pressure in the injection wells to avoid increasing the risk of flooding and damaging the confining clay layer. On the other hand, it must be able to sustain all pumping wells with a sufficiently high pumping rate as the pumping wells will operate close to their maximum capacity. This is related to the superposition principle in a confined aquifer implying that the resulting drawdown at a location is the algebraic sum of the effect of multiple pumping/injection wells in the neighbourhood. In addition, since the available area is limited to the campus, different well arrangements were tested for a short period of time (6 months – 2 years) and evaluated to effectively store heat while using the available space efficiently.

When a suitable arrangement was found, this scenario was evaluated for a period of 20 years (Fleuchaus et al., 2020). Within each year warm water injection is assumed to take place in summer (6 months) and cold water injection is assumed to take place in winter (6 months), both at the maximum rate. These long periods represent an extreme scenario. The temperature of the injected water was imposed in the model while the temperature of the extracted water varies according to heat transport processes. The injection temperature is normally approximately +5 °C for the warm well area and -5 °C for the cold well area (relative to the natural groundwater temperature of 13.8 °C). Furthermore, a yearly balance between heating and cooling demand from the underground was assumed.

4 Results

4.1 Hydraulic conditions for the ATES system

The maximum pumping rate in the currently available wells Yd 4 and Yd 6 was estimated to be respectively 4 and 1 m^3/h. According to Lebbe et al. (1992), a pumping rate of 1.66 m^3/h could be reached in PP 2, while we were limited to a rate of 1 m^3/h by our equipment.

During the pumping/injection test, the drop in water level due to pumping in Yd 4 could be observed in the pumping layer itself but also in Yd 6 (Fig. 5). In Yd 2, no drop in water level could be observed. This drop in water level illustrates that the semi-pervious layer Yd 5 does not prohibit the connection between Yd 6 and Yd 4 so the two layers cannot be considered as separate units. In contrast, the fact that no drop in water level could be observed illustrates the confining nature of Yd 3. This is confirmed by the observed influence of the injection. The injection in PB JE started shortly after the pumping was initiated. Despite the fact that PB JE is filtered from the top of Yd 6 to the bottom of Yd 1 (Fig. 3), the influence of the injection was only clearly visible in Yd 2 (Fig. 5).

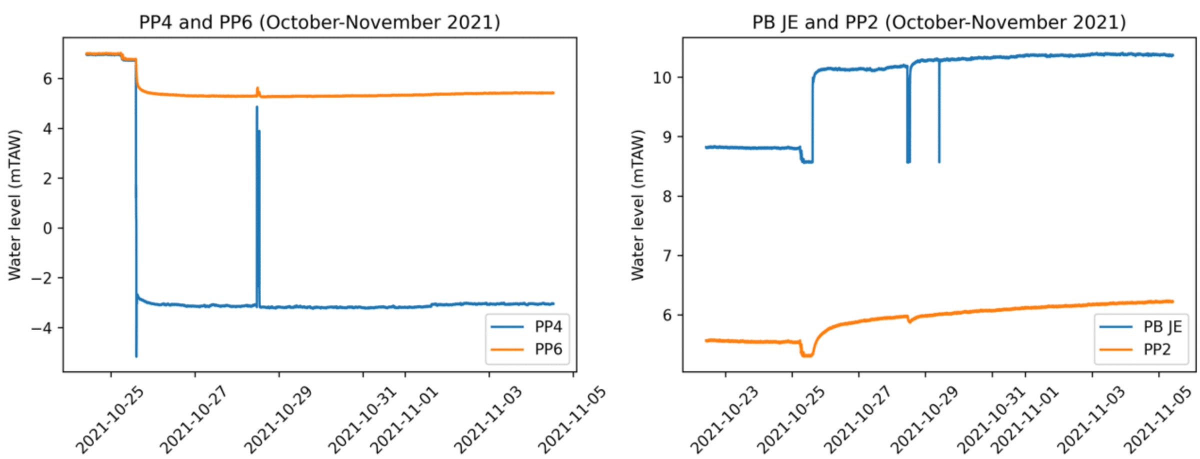

Fig. 5. Results of the pumping tests carried out on Campus Sterre (the peaks can be attributed to the disruption of the measurements to carry out the MFI tests).

Considering the absence of a pumping well with filter screens in all three pervious layers, the maximum pumping rate in the layered aquifer had to be estimated by means of the principle of superposition. This principle assumes that each pervious layer is fully confined (thus isolated from each other). On the one hand, this assumption seems acceptable for Yd 2 and Yd 4. On the other hand, it was shown that a strong connection between Yd 4 and Yd 6 exists indicating that Yd 5 is not a good confining layer. Hence, the maximum pumping rate in Yd 6 and Yd 4 combined is most likely smaller than the sum of their individual rates. Assuming that PP 6 can only account for 10 % of its estimated maximum pumping rate (i.e. 0.1 m^3/h), a total maximum pumping rate of 5.76 m^3/h was estimated in a fully screened well in the layered aquifer. It is however not recommended to exploit a well at the maximum rate, especially for a long period of time such as in an ATES system. Therefore the rate will be limited to 5 m^3/h for the rest of the study.

The maximum injection rate in the fully penetrating well PB JE was estimated to be 3.8 m^3/h. Using this constant injection rate for a continuous period of about two weeks no flooding of the surface was observed. The sudden decrease in injection capacity after these two weeks is most probably caused by trapped air which entered the well after problems with the pump, reducing the permeability. Injection of air is not expected to happen in the actual ATES system as the pressure in the system will always be maintained by a controlled valve at the injection.

The injection well PB JE was the limiting factor during the field test as it was constructed as a piezometer with a small diameter, not as a pumping or injection well. The current maximum injection rate was estimated at 3.8 m^3/h with a water level reaching the surface. A higher rate would probably be reached when using injection wells in a better state and with a larger diameter. So most likely the estimated maximum rate of 5 m^3/h can also be used for reinjection.

The injection capacity was also determined by the MFI tests. No sand could be visibly observed in the mesh netting. The slope for the two tests was 5.2 and 8.3 respectively. The filters of both MFI tests were visibly still relatively clean, which is a good indicator that the low MFI values measured are reliable. During the long-term injection, no decrease of injection capacity with time was observed, confirming that the risk of clogging should be limited.

4.2 Model validation

As mentioned earlier, the already calibrated model parameters of Lebbe et al. (1992) were used for the model created for this project. A good agreement with the triple pumping test data was observed indicating that the new numerical model is a good proxy for the model of Lebbe et al. (1992).

Using the same model parameters, the simulated drawdowns were compared to the drawdowns observed during the pumping and injection tests that were carried out for this project (Fig. 6). In general, when the injection is implemented, it becomes more difficult to simulate the observations. There is a good agreement in Fig. 6 for the observation wells (PB x.y) but there remains a discrepancy for the pumping/injection wells (PP x and PB JE). When considering a logarithmic time scale, the observed and the simulated drawdowns are however relatively parallel, indicating they are characteristic of a reservoir with similar properties (Cooper and Jacob, 1953).

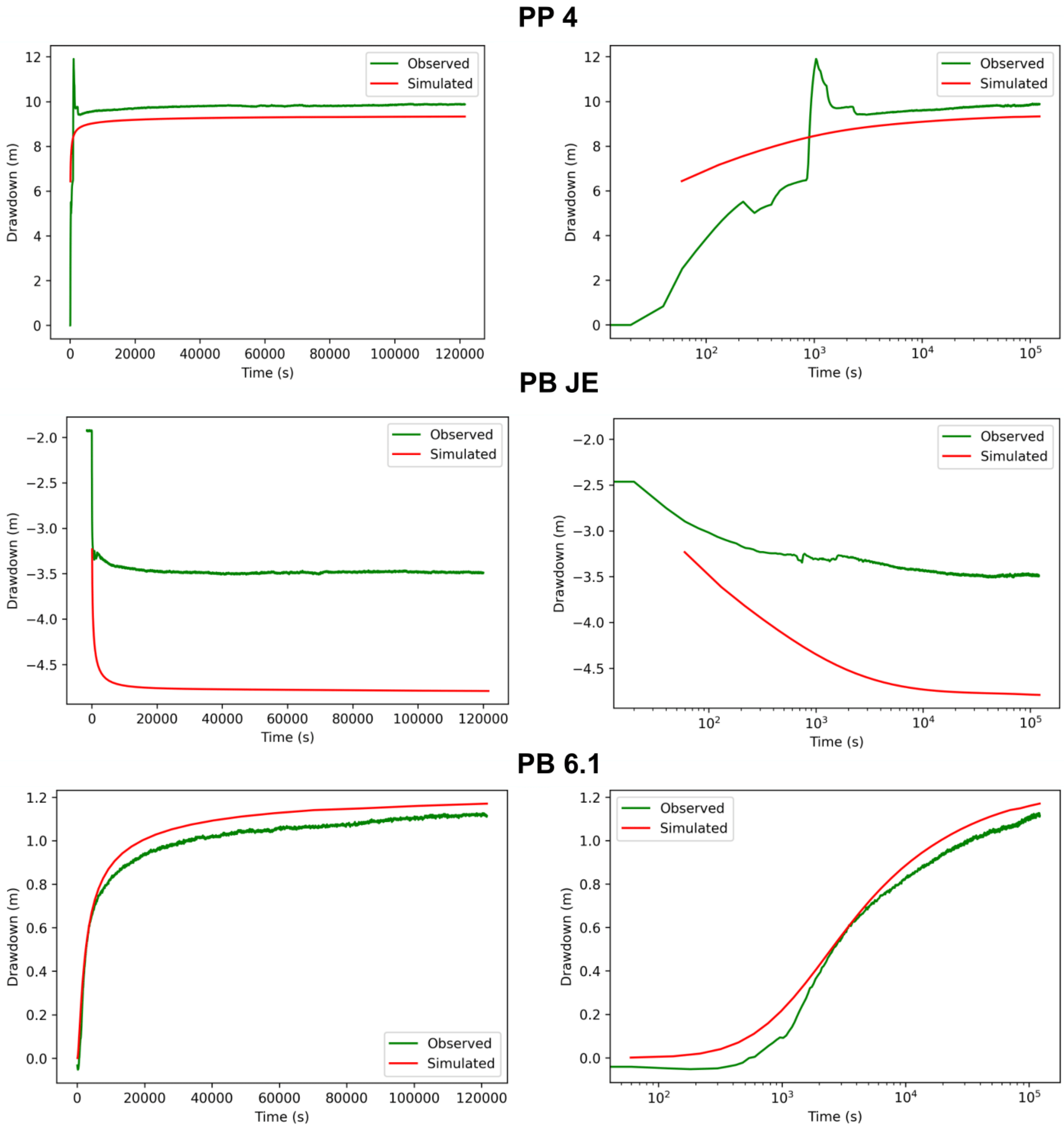

Fig. 6. Comparison of the simulated to the observed drawdown in PP 4, PB JE and PB 6.1. The drawdown is positive when the water level decreases and negative when the water level increases. On the right side, this is plotted using a logarithmic time.

The simulated pressure at the bottom of the well is too high compared to the observed one. This deviation can likely be attributed to the imperfect sealing of the semi-pervious layers during completion (Lebbe et al., 1992). The discrepancy at the injection well is larger, and we attribute it to the difficulty to model well behaviour..

Modeling a pumping/injection well is not straightforward as the detailed set-up of the well (bentonite seal, gravel pack, inner tube) is almost impossible to implement explicitly in

Modflow. The size of the discretization grid was reduced to a size close to the well diameter, approximating the dimensions of the well in the grid (Klepikova et al., 2016). The presence of water in the well instead of sediment was simulated by setting a very high value of the hydraulic conductivity (vertical and horizontal), decreasing the water pressure at the well when simulating injection. Nevertheless, the positive skin factor, which is a reduction of the permeability in the immediate vicinity of the well due to drilling/well completion/production processes, was not implemented in the model (Van Everdingen, 1953). In general, by reducing the permeability, the drawdown in the well itself would be larger and the cone of depression would be steeper. As such, at the pumping well PP 4, a positive skin factor could be present, this causes the observed drawdown to be larger than the simulated one as observed in **Error! Reference source not found.** 6. At the injection well PB JE, a positive skin factor would cause the negative drawdown to be larger (in absolute values) than the simulated one. However, the opposite is observed (Fig. 6). Although a negative skin factor could be present, as a gravel pack is present over the whole thickness of the aquifer including around semi-pervious layers, we rather think the discrepancy is related to an inadequate representation of the injection well in the model, which is corroborated by the higher discrepancy compared to PP 4. Since the model was initially calibrated by the pumping test as a homogenous aquifer, heterogeneity could also explain the difference: a higher hydraulic conductivity in the vicinity of PB JE would reduce the simulated pressure increase. However, including lateral heterogeneity at this stage would be highly speculative as the test zone is not representative of the whole modelled area.

Therefore, the model was considered valid for simulating the ATES scenarios, noting that the simulated pressure is likely overestimated in both the pumping and injection wells. The maximum pumping and injection rates were assumed to be 5 m^3/h based on the field observations.

4.3 ATES well arrangement

Considering the power requirement of 0.63 MW, ignoring in first instance the coefficient of performance, and a standard temperature difference between the extracted and the injected water of 5 °C, the required total pumping rate was estimated to be 108.62 m^3/h (equation 5). Assuming a pumping rate of 5 m^3/h per well pair, this results in the need for 22 well pairs and hence 44 wells. This exploitation flow rate is significantly below the usual pumping rate per well which is used in operating ATES systems (Table 3).

Table 3. Examples of operating ATES systems with their respective pumping rate per well (created after Abuasbeh and Acuña, 2018 [(1)]; Fleuchaus et al., 2018 [(2)]; Hoes et al., n.d. [(3)])

Project type	Location	Number of well pairs	Pumping rate per well (m^3/h)
Office buidlings [(1)]	Stockholm - Sweden	2	26
ETAP project [(3)]	Malle - Belgium	1	90
Project public hospital St-DIMPNA [(3)]	Geel - Belgium	1	100
Ikea [(2)]	Amersfoort - Netherlands	1	200
University campus [(2)]	Eindhoven - Netherlands	18	125
District heating [(2)]	Rostock - Germany	1	15
hospital KLINA project [(2,3)]	Brasschaat - Belgium	1	100
expo buidling [(2)]	Malmo - Sweden	5	24
museums quarter [(2)]	Greenwich - UK	1	45

Next, the hydraulic and thermal radius of influence were estimated in unit Yd 4 as it is the most permeable. This was calculated analytically taking into account a drawdown of 1.56 m at a distance of 5 m from the well as was indicated by a simulation of 6 months, resulting in a radius of influence of 36 m. Accounting for the thermal retardation factor of 1.83 (equation 4), the thermal radius of influence in Yd 4 is about 20 m. This estimation was also confirmed by the model.

Considering the guidelines for well placement drawn up by Bloemendal et al. (2018), first, a well arrangement in two clusters (i.e. one group of cold wells and one group of warm wells) was simulated (Fig. 7), allowing to minimize the space occupied by the ATES system, using the existing buildings as a constraint. However, this configuration yields a total absolute increase in water level in the injection cluster of about 53 m, while the drawdown resulting from a cluster of pumping wells is 46 m. Those high values resulting from the interactions between the wells in the same cluster working at rates close to the maximum rate (superposition effect) are too large and not sustainable in practice. Other clustered well arrangements were tested, but the simulated (negative and positive) drawdown remained too high (Fig. 7), indicating that the hydraulic conditions, rather than the thermal conditions, constitute the main limiting factor in this case.

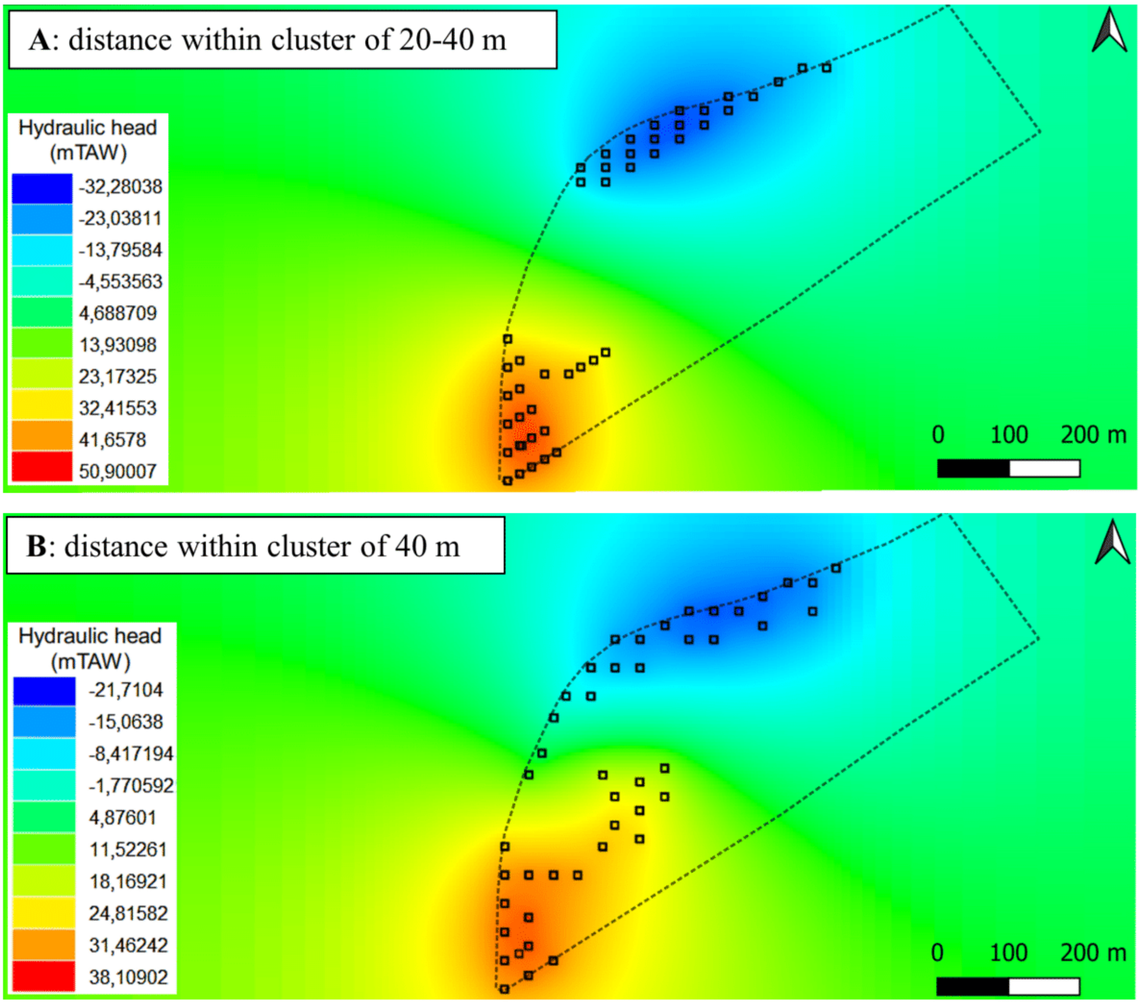

Fig. 7. Hydraulic head distribution after 6 months for different well arrangements. The dotted line indicates Campus Sterre.

Alternatively, a well configuration in lanes (alternating injection and pumping wells) was tested. This configuration should effectively limit the drawdown and hence also the injection pressure by the principle of superposition. Taking into account the thermal radius of influence of 20 m and the guidelines for placement drawn up by Bloemendal et al. (2018), the distance between the lanes should be at least 50 m. It was shown that a thermal breakthrough between the warm and cold well area was established within the first 6 months of operation which implies that the distance between the lanes was too small. Consequently, the distance between the lanes was incrementally adjusted up to 90 m to avoid a thermal breakthrough. This configuration reduced the drawdown and the injection pressure, but the maximum increase of 15 m was still too high (Fig. 8).

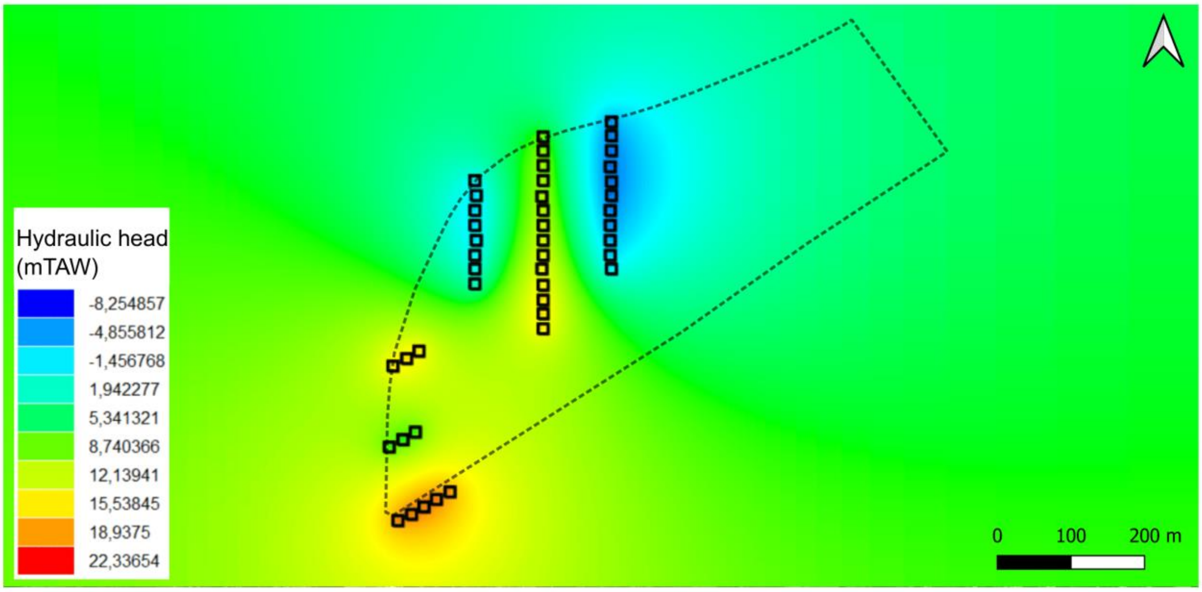

Fig. 8. The resulting hydraulic head for the lane-type arrangement with a distance between the wells within the lanes of 20 m and a distance in between the lanes of 90 m.

Nevertheless, since from a thermal point of view, no breakthrough occurred after the initial cycle, this well configuration was tested for 20 years to determine the storage efficiency of the ATES system.

The maximum temperature of the cold well area decreases with time to roughly 10.5 °C while the minimum temperature of the warm well area increases to roughly 17 °C (Fig. 9). The minimum temperature difference between the warm well area and the cold well area also increases with time, from approximately 8.5 to 9.5 °C, indicating that the storage is efficient and no thermal breakthrough occurs. For the latter, a difference between the seasons of roughly 0.5 °C can be observed. There is also a limited difference in temperature between the observation locations in the NE and SW, related to the inhomogeneity of the layer thickness.

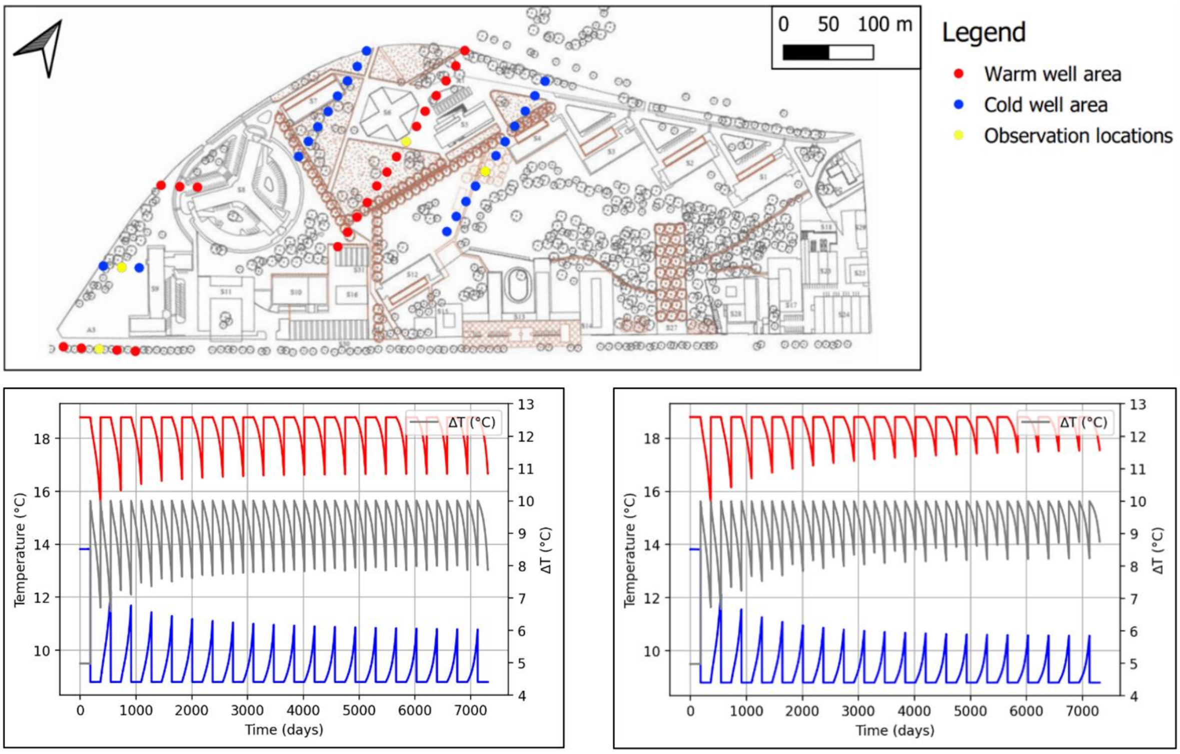

Fig. 9. On top: observation locations. Below: the temperature at the warm well area (red), the cold well area (blue), and the temperature difference (grey) after 20 years at the observation locations in the NE of the well area (left) and the SW of the well area (right).

Because of the relatively low hydraulic capacity of the aquifer, a high amount of well pairs is needed for the ATES system. These wells, placed in different clusters, interact with each other. This effect is most visible within the same cluster and leads to high pressures or drawdowns. The pressures might be too high for the confining clay layer to sustain, hence increasing the risk of soil outbursts (or flooding). To overcome this issue, an additional scenario was simulated using a well configuration in a checkerboard pattern. In this pattern, the injection and extraction wells are alternating, constituting the best option to limit the change in the hydraulic head in the aquifer, but it could reduce the thermal efficiency. The wells were placed as far as possible from each other, within the available space of Campus Sterre. This results in a well spacing of minimum 80 m. With this configuration, the maximum hydraulic head while injecting remained limited (15 mTAW, or 5 m above the ground surface) as was the case for a single pair (Fig. 10).

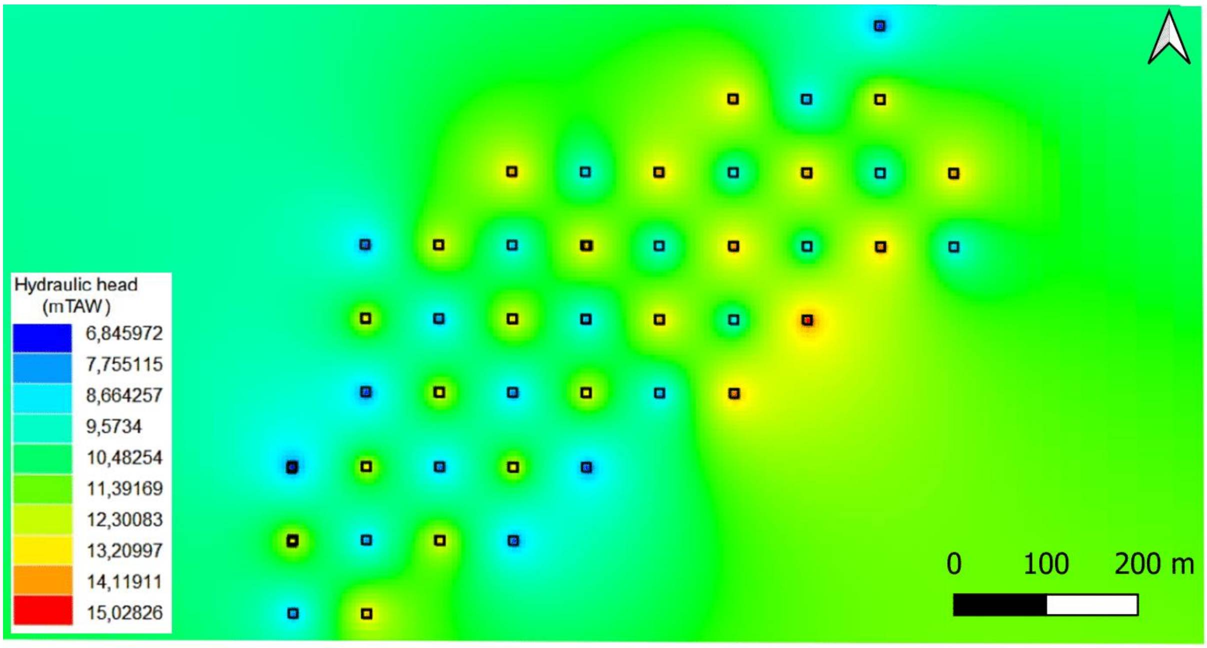

Fig. 10. Hydraulic head distribution after a simulation period of 20 years in a checkerboard pattern.

Fig. 11 also shows that the minimum temperature of the warm well area increases while the maximum temperature of the cold well area decreases. The system is therefore thermally efficient, although the temperature difference is, as expected, slightly lower than in the previous scenario. As the maximum temperature difference is roughly twice as large as the initially estimated 5 °C, the maximum produced power was also estimated to be about twice the power requirement of this project (2 · 0.63 MW). Next, the extracted thermal energy per season (integration over 6 months for heating or cooling) was calculated based on the temperature difference in Fig. 11 and the extraction rate (Fig. 12). The initially estimated power demand for this project was based on cumulative energy demand of 1.5 GWh with a peak cooling demand in summer. Fig. 12 shows that the simulated energy output is 3 times as large. However, as long winter and summer seasons (6 months) are simulated in which the system operates at its maximum flowrate and thus power, it must be emphasized that the simulated scenario represents the maximum upper limit for energy production.

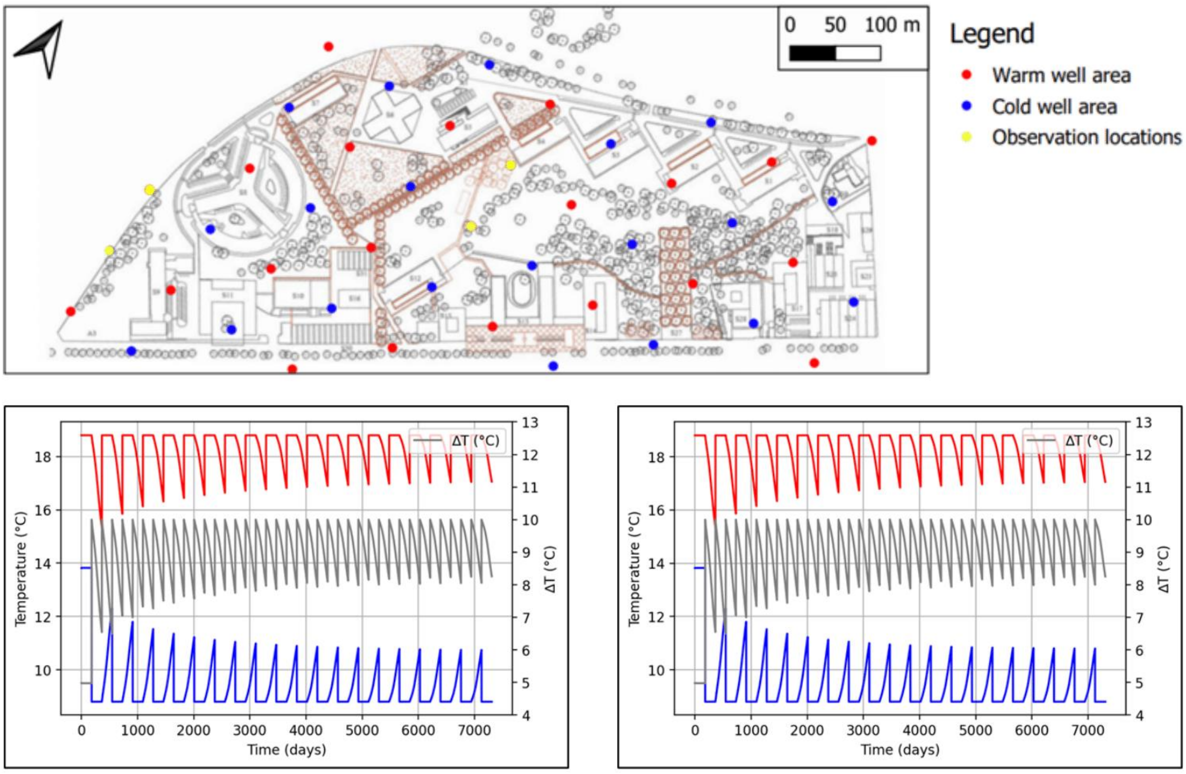

Fig. 11. On top: observation locations. Below: the temperature at the warm well area (red), the cold well area (blue), and the temperature difference (grey) after 20 years at the observation locations in the NE of the well area (left) and the SW of the well area (right).

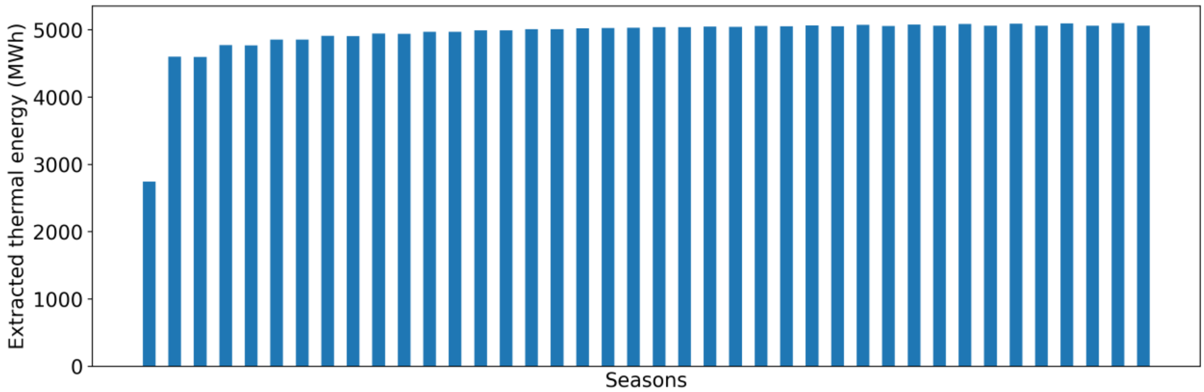

Fig. 12. Energy output per season (6 months) based on the simulation of an ATES system in a checkerboard pattern for 20 years.

5 Discussion

The field tests and initial modeling results have validated that the low transmissivity aquifer located on Campus Sterre could only sustain a maximum pumping and injection rate of about 5 m³/h. This limiting extraction rate results in new constraints for the arrangement of the ATES wells.

Arranging the wells in 2 large clusters as was first done in Fig. 7 is not a feasible option for the future ATES project considering the excessive drawdowns. This results from the principle of superposition which implies that the resulting hydraulic head at a certain location is the combination of all influences (resulting from different pumping/injection wells) at that same location. When many wells are grouped into one cluster with an inter-well distance which is less than the hydraulic radius of influence, this will result in an excessive drawdown (positive or negative), especially in a configuration where the extraction rate is close to the maximum yield. Even though the model tends to overestimate the injection pressure, an increase in water level of minimum 31 m relative to the natural groundwater level is not acceptable. Using such a configuration, flooding will likely occur around the injection wells and the relatively thin confining clay layer might not be able to withstand such high pressures. Also, the minimum drawdown of about 28 m at the pumping wells is not feasible. This would probably cause the aquifer to become partly unsaturated and consequently the necessary pumping rate of 5 m^3/h per well could not be reached anymore.

Next, the arrangement of wells in several lanes showed that a distance of 90 m between the lanes was necessary to avoid a thermal breakthrough. This is significantly larger than the guidelines Bloemendal et al. (2018) proposed. Because of the superposition effect of multiple wells, the radii of influence which were deduced for a single well pair are not valid anymore for clusters or lanes. These configurations result in an increased gradient between warm and cold wells which speeds up groundwater flow. The lane arrangement showed an overall improvement in the calculated drawdown at the location of the injection wells due to the closeness of the pumping wells. However, it also showed that the hydraulic head in the SW of the well area is significantly higher than in the NE. It might be the result of the fact that the warm lanes in the SW are not located in between two cold lanes which counterbalances the increase in hydraulic head.

From a thermal point of view, no thermal breakthrough occurred if the distance between the wells was large enough. In this case, the safe distance was 4.5 times larger than the thermal radius calculated for one well pair. As expected, the thermal efficiency increases with time as illustrated by the minimum temperature difference between warm and cold wells. A seasonal variation of about 0.5 °C remains within realistic limits. The small difference between the temperature at the observation locations in the NE and SW might be explained by the fact that in the NE the lanes consist of more wells close to each other, slightly decreasing the storage efficiency.

Our investigations demonstrate that the injection pressure is the main limiting factor in the design of this particular ATES system. It is not surprising as the pumping/injection rate (5 m^3/h) is close (86%) to the estimated maximum rate for this aquifer (about 5.8 m^3/h). Consequently, a well arrangement in a checkerboard pattern is the best approach to limit the increase in hydraulic head in injection wells. However, this pattern is less optimal as it utilizes all the available space and hence less cost-efficient when considering the piping and installation costs. The total costs of installation for such an ATES system would nevertheless remain much smaller than the foreseen BTES system (about 50% of the BTES costs).

In terms of thermal efficiency, it might also increase the risk of a thermal breakthrough as cold and warm wells are alternating. However, as the injection pressure is more limited, it reduces the effective thermal radius. The diagonals in the checkerboard pattern actually resemble the lane-type well arrangement but with a larger distance between wells of the same cluster (lane), confirming that the hydraulic interaction is the main limiting factor for low transmissivity ATES systems. Such a configuration can easily be adapted to accommodate the buildings and optimize the usage of the available space. Because of the limited hydraulic interaction, the distance between the wells might be decreased to about 60 m without significantly increasing the risk of thermal breakthrough.

The average low permeability of the study area limits the thermal radius for one well pair. However, when placing several wells at a relatively short distance from each other in a lane, the injection pressure, and hence also the thermal radius, increased. As such, this shows that the low permeability in the study area is neither an advantage nor a disadvantage for the ATES system. Furthermore, it was proven that the hydraulic radius of influence is more limiting than the thermal radius of influence. As such, it is suggested to use the former to apply the guidelines for the well placement drawn up by Bloemendal et al. (2018) when looking to further optimize the well configuration.

Although we demonstrated an ATES system should be sustainable on campus Sterre, there are still some challenges and uncertainties which need to be further investigated:

1. As the pumping rate of 5 m^3/h was an estimate based on field experiments using the available wells and analytical approximations using the principle of superposition, this flow rate still needs to be confirmed in the field using a newly constructed well pair with optimally placed filters in the three pervious layers. These wells would have a large diameter and should be thoroughly developed to reduce well losses.
2. To improve the model and optimize the efficiency of the system, heat losses at the surface should be introduced in the model by adapting the boundary conditions for heat transport.
3. The hydraulic conductivity and storage coefficient for all layers were already accurately estimated by Lebbe et al. (1992) who also carried out a thorough analysis of the results. However, a detailed sensitivity analysis should be carried out for the porosity and thermal parameters. Heat tracer experiments could also be carried out to validate the porosity and thermal parameters (e.g. Wildemeersch et al., 2014). Next to this, a thermal response test can be carried out to validate the thermal conductivity of the subsurface.
4. Because of the limited size of the zone investigated by the field tests, homogeneous parameters within each layer were used for the groundwater models. This is likely an

oversimplification and should be investigated. Heterogeneity is known to influence the efficiency of ATES systems (Possemiers et al., 2015; Sommer et al., 2013; Hermans et al., 2018, 2019). Similarly, the thickness and continuity of the confining layer throughout the campus should be confirmed. If it were partly absent, the studied aquifer layer would constitute an unconfined aquifer together with the quaternary layer, which would likely modify the hydraulic behaviour and the conclusion of the study.

6 Conclusion

A medium permeability aquifer with limited thickness located on Campus Sterre (Ghent, Belgium) was investigated as a possible candidate for aquifer thermal energy storage even though it is conventionally disregarded because of its limited transmissivity. Based on field experiments, it was shown that the maximum pumping and injection rate within this aquifer is only 5 m^3/h, which is much smaller than most operating ATES systems. Nevertheless, the aquifer seems suitable as the injection rate could be sustained for a long period of time, and no clogging of the injection well could be detected, which is one of the main concerns in a medium permeability aquifer.

For low transmissivity aquifers, the energy demand must be covered by increasing the number of well pairs, which results in new challenges for well placement. Based on the energy demand on the campus, an ATES system using 22 well pairs should be operated. Simulation with calibrated groundwater models showed that well arrangements in clusters or in lanes, based on estimation of the hydraulic and thermal radii from a single well pair, were not adequate because they were resulting in an excessive water pressure and drawdown in the injection and pumping zones respectively. This is a direct consequence of the superposition principle, as neighbouring wells interact with each other. Instead, the wells should be arranged in a checkerboard pattern of alternately warm and cold wells with each a pumping/injection rate of 5m^3/h. This configuration minimizes the hydraulic interaction while avoiding any thermal breakthrough. Although such an ATES system would operate in sub-optimal conditions, ATES is certainly an option to consider in comparison with BTES in a detailed design and cost analysis.

Our study shows that so far the potential of low transmissivity aquifer for ATES systems has likely been underestimated. With the increase in energy prices and the long-term objectives to reduce greenhouse gas emissions, the interest in ATES systems will likely increase in the future. In absence of accessible productive aquifers, either because of their absence or because they are used for drinking water production, low transmissivity aquifers can constitute suitable alternatives, although suboptimal. Their potential should be confirmed by more field studies targeting specifically ATES systems (long-term injection, clogging, heterogeneity).

Acknowledgements

This research was supported by the Ghent University Special Research Fund. We would like to express our sincere thanks and appreciation to Marieke Paepen and Robin Thibaut of the hydrogeology department for assisting with the field work and computer simulations.

References

Aalten, T., Witteveen, H., 2015. Protocol zand- en slibhoudendheidsmetingen, versie 1.0. BodemenergieNL. Last accessed May 19, 2022 from https://docplayer.nl/48776639-Protocol-zand-en-slibhoudendheidsmetingen.html

Abuasbeh, M., & Acuña, J., 2018. ATES system monitoring project, first measurement and performance evaluation: case study in Sweden. IGSHPA Research Track. Last accessed September 8, 2022 from https://shareok.org

Batac, K. I. T., Collera, A. A., Villanueva, R. O., & Agaton, C. B., 2022. Decision Support for Investments in Sustainable Energy Sources Under Uncertainties. International Journal of Renewable Energy Development, 11(3), 801-814. DOI: https://doi.org/10.14710/ijred.2022.45913

Bayer, P., Saner, D., Bolay, S., Rybach, L., Blum, P., 2012. Greenhouse gas emission savings of ground source heat pump systems in Europe: A review. Renew. Sustain. Energy Rev. 16, 1256–1267. doi:10.1016/j.rser.2011.09.027

Bedekar, V., Morway, E.D., Langevin, C.D., and Tonkin, M., 2016. MT3D-USGS version 1.0.0: Groundwater Solute Transport Simulator for MODFLOW: U.S. Geological Survey Software Release, 30 September 2016. Last accessed May 19, 2022 from http://dx.doi.org/10.5066/F75T3HKD

Bloemendal, M., Olsthoorn, T., & van de Ven, F., 2015. Combining climatic and geo-hydrological preconditions as a method to determine world potential for aquifer thermal energy storage. Science of the Total Environment, 538, 621–633. https://doi.org/10.1016/j.scitotenv.2015.07.084

Bloemendal, M., 2018. The hidden side of cities: Methods for governance, planning and design for optimal use of subsurface space with ATES. PhD thesis, Delft University of Technology. Last accessed May 19, 2022 from https://doi.org/10.4233/uuid:0c6bcdac-6bf7-46c3-a4d3-53119c1a8606

Bloemendal, M., Olsthoorn, T., 2018. ATES systems in aquifers with high ambient groundwater flow velocity. Geothermics, 75 (January), 81–92. Last accessed May 19, 2022 from https://doi.org/10.1016/j.geothermics.2018.04.005

Bloemendal, M., Jaxa-Rozen, M., Olsthoorn, T., 2018. Methods for planning of ATES systems. Applied Energy, 216, 534–557. Last accessed May 19, 2022 from https://doi.org/10.1016/j.apenergy.2018.02.068

Cooper, H.H., Jacob, C.E., 1953. A generalized graphical method of evaluating formation constants and summarizing well-field history. Groundwater notes hydraulics, No. 7, 90-102. Last accessed March 31, 2022 from https://www.nrc.gov/docs/ML1429/ML14290A600.pdf

Databank Ondergrond Vlaanderen (DOV) – Vlaamse Overheid. (n.d.). Verkenner. Last accessed April 19, 2022 from https://www.dov.vlaanderen.be/portaal/?module=verkenner

De Zwart, A.H., 2007. Investigation of clogging processes in unconsolidated aquifers near water supply wells. Proefschrift. Hydrology and Ecology Section and Petroleum Engineering Section, Department of Civil Engineering and Geosciences, Delft University of Technology. Last accessed May 19, 2022 from https://repository.tudelft.nl

Dupuit, J.É.J., 1863. Études Théoriques et Pratiques sur le Mouvement des Eaux Dans les Canaux Découverts et à Travers les Terrains Perméables: Avec des Considérations Relatives au Régime des Grandes Eaux, au Débouché à leur Donner, et à la Marche des Alluvions dans les Rivières à Fond Mobile; Dunod: Paris, France, 1863.

European Commission, 2012. Roadmap 2050 Low Carbon Europe. Last accessed May 19, 2022 from https://doi.org/10.2833/10759

European Commission, 2019. Heating and cooling. Comprehensive assessment. https://ec.europa.eu/energy/en/topics/energy-efficiency/heating-and-cooling

Fleuchaus, P., Godschalk, B., Stober, I., Blum, P., 2018. Worldwide application of aquifer thermal energy storage – A review. Renewable and Sustainable Energy Reviews, 94(November 2017), 861–876. Last accessed May 19, 2022 from https://doi.org/10.1016/j.rser.2018.06.057

Fleuchaus, P., Schüppler, S., Godschalk, B., Bakema, G., Blum, P., 2020. Performance analysis of Aquifer Thermal Energy Storage (ATES). Renewable Energy, Volume 146 (February 2020), pp. 1536-1548. Last accessed May 19, 2022 from https://doi.org/10.1016/j.renene.2019.07.030

Gao, Q., Zhou, X.Z., Jiang, Y., Chen, X.L., Yan, Y.Y., 2013. Numerical simulation of the thermal interaction between pumping and injecting well groups. *Applied Thermal Engineering*, *51*(1–2), 10–19. Last accessed May 19, 2022 from https://doi.org/10.1016/j.applthermaleng.2012.09.017

Glassley, W.E., 2015. Geothermal energy: Renewable energy and the environment, Third edition. CRC Press, inc.

Hecht-Méndez, J., Molina-Giraldo, N., Blum, P., Bayer, P., 2010. Evaluating MT3DMS for heat transport simulation of closed geothermal systems. *Ground Water*, *48*(5), 741–756. Last accessed May 19, 2022 from https://doi.org/10.1111/j.1745-6584.2010.00678.x

Hecht-Méndez, J., de Paly, M., Beck, M., & Bayer, P., 2013. Optimization of energy extraction for vertical closed-loop geothermal systems considering groundwater flow. Energy Conversion and Management, 66, 1–10. https://doi.org/10.1016/j.enconman.2012.09.019

Hermans, T., Nguyen, F., Klepikova, M., Dassargues, A., Caers, J., 2018. Uncertainty Quantification of Medium-Term Heat Storage From Short-Term Geophysical Experiments Using Bayesian Evidential Learning. Water Resources Research, 54(4), 2931–2948. Last accessed May 19, 2022 from https://doi.org/10.1002/2017WR022135

Hermans, T., Lesparre, N., De Schepper, G., & Robert, T., 2019. Bayesian evidential learning: a field validation using push-pull tests. Hydrogeology Journal, 27(5), 1661–1672. https://doi.org/10.1007/s10040-019-01962-9

Hoes, H., Desmedt, J., Robeyn, N., & van Bael, J., n.d. Experiences with ATES applications in Belgium. Operational results and energy savings. Flemish Institute for Technological Research 'VITO'. Last accessed September 8, 2022 from https://www.researchgate.net/publication/237401555

Jenne, E., Andersson, O., Willemsen, A., 1992. Well, hydrology, and geochemistry problems encountered in ATES systems and their solutions. SAE Technical Paper (1992). Last accessed May 19, 2022 from https://www.osti.gov/servlets/purl/10187570

Kim, J., Lee, Y., Yoon, W.S., Jeon, J.S., Koo, M.H., Keehm, Y., 2010. Numerical modeling of aquifer thermal energy storage system. *Energy*, *35*(12), 4955–4965. Last accessed May 19, 2022 from https://doi.org/10.1016/j.energy.2010.08.029

Klepikova, M., Wildemeersch, S., Hermans, T., Jamin, P., Orban, P., Nguyen, F., et al., 2016. Heat tracer test in an alluvial aquifer: Field experiment and inverse modeling. *Journal of Hydrology*, *540*, 812–823. https://doi.org/10.1016/j.jhydrol.2016.06.066

Langevin, C.D., Thorne, D.T., Dausman, A.M., Sukop, M.C., Guo, W., 2007. SEAWAT Version 4: A Computer Program for Simulation of Multi-species Solute and Heat Transport, US Geol. Surv. Tech. Methods, Book 6, US Geological Survey Reston, VA (Chapter A22). Last accessed May 19, 2022 from https://doi.org/10.3133/tm6A22

Langevin, C.D., Hughes, J.D., Banta, E.R., Niswonger, R.G., Panday, S., Provost, A.M., 2017a. Documentation for the MODFLOW 6 Groundwater Flow Model: U.S. Geological Survey Techniques and Methods, book6, chapter A55, 197p. Last accessed May 19, 2022 from https://doi.org/10.3133/tm6A55

Langevin, C.D., Hughes, J.D., Banta, E.R., Provost, A.M., Niswonger, R.G., and Panday, S., 2017b. MODFLOW 6 Modular Hydrologic Model: U.S. Geological Survey Software. Last accessed May 19, 2022 from https://doi.org/10.5066/F76Q1VQV

Lebbe, L., Mahauden, M., De Breuck, W., 1992. Execution of a triple pumping test and interpretation by an inverse numerical model. International Journal of Applied Hydrogeology, volume 1 4/1992, pp. 20-34.

Olsthoorn, T.N., 1982. The clogging of recharge wells, main subjects; KIWA Communications 72, Rijkswijk. Last accessed May 19, 2022 from https://library.wur.nl/WebQuery/hydrotheek/2108784

Perego, R., Viesi, D., Pera, S., Dalla, G., Cultrera, M., Visintainer, P., Galgaro, A., 2020. Revision of hydrothermal constraints for the installation of closed-loop shallow geothermal systems through underground investigation , monitoring and modeling. Renewable Energy, 153, 1378–1395. Last accessed May 19, 2022 from https://doi.org/10.1016/j.renene.2020.02.068

Pollock, D.W., 2012. User Guide for MODPATH Version 6 – A Particle-Tracking Model for MODFLOW. US Geol. Surv. Techniques and Methods 6 – A41. Last accessed May 19, 2022 from https://doi.org/10.3133/tm6A41

Possemiers, M., 2014. Aquifer thermal energy storage under different hydrochemical and hydrogeological conditions. PhD Thesis, Faculty of Science, KU Leuven. Last accessed May 19, 2022 from https://limo.libis.be

Possemiers, M., Huysmans, M., Batelaan, O., 2015. Application of multiple-point geostatistics to simulate the effect of small scale aquifer heterogeneity on the efficiency of aquifer thermal energy storage. Hydrogeology Journal, 23(5), 971–981. Last accessed May 19, 2022 from https://doi.org/10.1007/s10040-015-1244-3

Ramos-Escudero, A., García-cascales, M.S., Cuevas, J.M., Sanner, B., Urchueguía, J.F., 2021. Spatial analysis of indicators affecting the exploitation of shallow geothermal energy at European scale. Renewable Energy, 167, 266–281. Last accessed May 19, 2022 from https://doi.org/10.1016/j.renene.2020.11.081

Schippers, J.C., Verdouw, J., 1979. De membraanfiltratie-index als kenmerk voor de filtreerbaarheid van water. H2O (12), nr.5, pp 104-109. Last accessed May 19, 2022 from https://edepot.wur.nl/398518

Schippers, J.C., Verdouw, J., 1980. The Modified-Fouling Index. A method for Determining the Fouling Characteristics of Water. Desalination 32, pp 137-148. Last accessed May 19, 2022 from https://doi.org/10.1016/S0011-9164(00)86014-2

Sommer, W., Valstar, J., Van Gaans, P., Grotenhuis, T., & Rijnaarts, H., 2013. The impact of aquifer heterogeneity on the performance of aquifer thermal energy storage. Water Resources Research, 49(12), 8128–8138. Last accessed May 19, 2022 from https://doi.org/10.1002/2013WR013677

Thiem, G., 1906. Hydrologische Methoden: Dissertation zur Erlangung der Wurde eines; JM Gebhardt: Leipzig, Germany, 1906.

Vandenbohede, A., Hermans, T., Nguyen, F., Lebbe, L., 2011. Shallow heat injection and storage experiment: Heat transport simulation and sensitivity analysis. Journal of Hydrology, 409(1–2), 262–272. Last accessed May 19, 2022 from https://doi.org/10.1016/j.jhydrol.2011.08.024

Van Everdingen, A.F., 1953. The Skin Effect and Its Influence on the Productive Capacity of a Well. Journal of Petroleum Technology, 5(06), 171–176. Last accessed May 19, 2022 from https://doi.org/10.2118/203-g

Wildemeersch, S., Jamin, P., Orban, P., Hermans, T., Klepikova, M., Nguyen, F., Brouyère, S., Dassargues, A., 2014. Coupling heat and chemical tracer experiments for estimating heat transfer parameters in shallow alluvial aquifers. Journal of Contaminant Hydrology, 169, 90–99. https://doi.org/10.1016/j.jconhyd.2014.08.001

Winston, R.B., 2019. ModelMuse version 4—A graphical user interface for MODFLOW 6: U.S. Geological Survey Scientific Investigations Report 2019–5036, 10 p., Last accessed May 19, 2022 from https://doi.org/10.3133/sir20195036

WTCB, 2017. Code van goede praktijk. Ontwerp, uitvoering en beheer van KWO-systemin. Last accessed June 10 from https://www.techlink.be/media/647315/koude-warmteopslagsystemen.pdf.

Yapparova, A., Matthäi, S., Driesner, T., 2014. Realistic simulation of an aquifer thermal energy storage: Effects of injection temperature, well placement and groundwater flow. Energy, *76*, 1011–1018. Last accessed May 19, 2022 from https://doi.org/10.1016/j.energy.2014.09.018

Zheng, C., and Wang, P.P., 1999. MT3DMS: A modular three-dimensional multi-species transport model for simulation of advection, dispersion and chemical reactions of contaminants in groundwater systems; Documentation and user's guide: Contract report SERDP-99-1: U.S. Army Engineer Research and Development Center, Vicksburg, MS, 169 p. Last accessed May 19, 2022 from https://hydro.geo.ua.edu/mt3d/mt3dmanual.pdf

Zheng, C., 2010. MT3DMS v5.3: Supplemental User's Guide. Department of Geological Sciences The University of Alabama, 51. Last accessed May 19, 2022 from https://hydro.geo.ua.edu/mt3d/mt3dms_v5_supplemental.pdf